ICARUS 89, 93–112 (1991)

Rheological Properties of Ammonia–Water Liquids and Crystal–Liquid Slurries: Planetological Applications

J. S. KARGEL, S. K. CROFT, J. I. LUNINE, AND J. S. LEWIS

Lunar and Planetary Laboratory, University of Arizona, Tucson, Arizona 85721

Received April 25, 1990; revised August 24, 1990

The viscosities of aqueous mixtures plausibly representing a range of cryovolcanic substances seen on the icy satellites have been measured in the laboratory or obtained from literature sources. These viscosities range from 10^{-2} poise (pure water) to 10^{2} poises (ammonia–water peritectic) to about 10^{5} poises (ammonia–water–methanol peritectic). The viscosities of the liquid mixtures examined in this work are much greater than would be expected based on the assumption that the end member molecules are noninteractive. This observation supports others based on molar volumes and vapor pressure relations indicating that strong molecular interactive forces exist and have an important bearing on the physical properties of the mixtures. With supercooling and/or partial crystallization, these substances may attain viscosities several orders of magnitude greater than those given above. The rheological effects of partial crystallization parallel the same effects in silicate lavas, so it is reasonable to interpret cryovolcanic morphologies on the icy satellites in the same ways that we interpret remotely observed silicate volcanic morphologies on the Earth and terrestrial planets, after accounting for differences in surface gravities and lava densities, and allowing for uncertainties in surface slopes and extrusion rates. Given the wide range of viscosities for simple aqueous mixtures, and the rheological effects of realistic thermal states, the characteristics of observed cryovolcanic flows and resurfaced plains on the icy satellites can be understood within the framework of conventional magmatic processes working on exotic icy substances. © 1991 Academic Press, Inc.

1. INTRODUCTION

The reconnaissance of the Voyager spacecraft through the outer solar system revealed an unexpected diversity and intensity of internally driven modifications to the surfaces of icy satellites. Pre-Voyager theoretical arguments suggested that some of the icy satellites might have been volcanically ("cryovolcanically") active at some point, where the "lava" was water or some cryogenic liquid such as ammonia–water (Lewis 1972, Consolmagno and Lewis 1978). Voyager's observations have confirmed these early suspicions, but have further indicated that cryovolcanic processes are complex and varied and have combined with tectonic and other processes to produce a bewildering variety of bizarre landscapes, each unique in its own expression.

Our present understanding of icy satellites does not lend itself to a good predictive understanding of the geological styles of icy satellites. The genesis of the many distinctive landforms and landscapes must, however, relate in some way to important intersatellite variable parameters including satellite radius, surface gravity, rock : ice ratio, heat source, and ice composition. Ice and cryolava compositions and composition-dependent rheologies are likely to be of particular importance for satellites with histories of cryovolcanism. However, our present knowledge of solid–liquid phase equilibria and other physicochemical properties of volatile assemblages relevant to cryovolcanism lags at least 60 years behind our equivalent knowledge of silicate properties relevant to terrestrial igneous processes.

This report is the second from our group attempting to redress some important deficiencies. In an earlier paper we presented the equations of state for ammonia–water liquids (Croft *et al.* 1988). Here, we present rheological data for ammonia–water liquids and partially crystallized slurries and apply these data to matters pertaining to cryovolcanism. We extend our report to include ammonia–water–methanol liquids, taking methanol to be representative of many possible ammonia–water-soluble chemical components likely to be present in minor or trace amounts in icy satellites. (Other likely components include $(NH_4)_2S$, NH_4CN, $(CH_2)_6N_4$, NaCl, NH_4Cl, $(NH_4)_2SO_4$, amino acids, and many others; Kargel 1988, 1990.) We also summarize data from the literature for other substances so as to provide an overview of the extreme rheological range of plausible cryovolcanic agents.

Previous work on the viscosities of superliquidus ammonia–water liquids include two reports from the Russian literature (Pleskov and Igamberdyev 1939, Pinevich 1948) and, more recently, an abstract by McKinnon and Meadows (1984). The Russian workers were concerned with viscosities at temperatures above 200 K, although McKin-

0019-1035/91 $3.00

non and Meadows extrapolated their data down in temperature and through composition to the ammonia–water eutectic and estimated viscosities similar to those reported here from direct measurements.

2. EXPERIMENTAL

The rheologies of ammonia–water and ammonia–water–methanol liquids and liquid–crystal slurries were investigated using the falling sphere and rotating disk methods.

2.1 Rotational Viscometry

These measurements were obtained with an HB Model Brookfield viscometer. This instrument measures the resistance encountered by cylindrical and disk-like spindles rotating in a viscous medium contained in a coaxial cylindrical vessel. All of the measurements reported here were made with Brookfield's largest spindle ("HB1"). This spindle is classified as a disk spindle, although it actually is a short cylinder, 5.6 cm in diameter, 2.3 cm high, and mounted on a coaxial cylindrical shaft 0.3 cm in diameter. The geometry is rather complex, so the conversion from rotation rates and applied torque to absolute viscosities is by the manufacturer's calibration rather than from first principles.

Viscosity was measured as functions of temperature, composition, strain rate, and degree of partial crystallization (Table I). Measurements at three or more different spindle rotation rates for each composition and temperature allowed departures from Newtonian viscous behavior to be detected and quantified (Newtonian behavior was observed in all samples except for some partially crystallized slurries, as described below). For a consistent and simple presentation, all viscosities reported in Table I were either obtained with the spindle rotating at 20 revolutions per minute, or were reduced to 20 rpm using a power-law extrapolation or interpolation of data obtained at other rotation rates; to complete the rheological description of non-Newtonian slurries the power-law exponent, n, is also given in Table I (these details are irrelevant when the substance rheology is Newtonian, in which case $n = 1$ and the viscosity alone is sufficient to describe the rheology).

The range of reliable viscosities obtained with this instrument is from about 1 to 10^3 poises (10 poise = 1 Pa-sec). Instrumental precision may, in principle, approach 1% at full scale torque. In practice, measurements were repeatable to about ±3% to ±15%, 8% being most typical. These larger figures include the fact that torque was most typically not at full scale, and include uncertainties in the temperature and composition of the liquid (see below) as well as other experimental sources of error.

Each run used about 1400 ml of solution contained in a closed and insulated cylindrical polyethylene vessel with

TABLE I
Ammonia–Water Viscosities Obtained by Rotational Viscometry

Composition (wt.% NH_3)	Temperature (K)	% Crystallization	Viscosity (poise)	Power law exponent, n
12.4	254.05	5	2.0	1.6
12.4	252.95	9	2.4	1.4
12.4	249.95	16	8.0	1.8
12.4	248.95	18	7.6	1.9
12.4	245.55	26	10.1	1.5
14.0	251.15	2	1.0	1.9
14.0	249.75	6	1.4	2.1
14.0	244.95	18	3.0	1.8
14.0	244.15	19	4.0	2.1
18.1	240.05	5	9.2	1.7
18.1	238.95	7	12.0	2.1
18.1	233.35	12	22.0	2.2
18.1	231.45	17	44.0	1.9
18.1	227.55	21	63	1.8
18.1	221.15	25	77	2.2
21.6	226.95	6	2.6	2.1
21.6	224.55	8	3.6	2.1
21.6	220.45	13	4.6	2.2
21.6	213.45	18	15.4	2.4
21.6	199.55	25	51	1.9
25.2	214.75	3	2.6	1.6
25.2	211.65	5	6.2	1.8
25.2	206.15	9	12.4	1.6
25.2	199.35	13	17.0	1.3
26.7	209.65	0	1.2	1.0
26.7	204.35	5	6.6	1.4
26.7	195.65	10	15.0	1.2
28.4	207.85	0	1.2	—
28.4	202.85	0	2.0	1.0
28.4	199.85	1	2.8	1.0
28.4	196.65	3	5.3	1.1
28.4	191.45	6	13.6	1.2
28.4	184.65	10	40.0	1.2
28.4	183.75	10	40.0	1.2
29.4	209.15	0	1.0	—
29.4	205.75	0	1.4	—
29.4	205.45	0	1.3	—
29.4	202.85	0	1.8	—
29.4	202.55	0	1.8	—
29.4	198.95	0	3.0	—
29.4	198.05	0	3.2	1.0
29.4	197.55	0	3.3	1.0
29.4	197.35	0	4.0	—
29.4	196.35	0	4.2	1.0
29.4	195.75	0	4.8	1.0
29.4	193.05	2	7.2	1.0
29.4	192.15	2	8.2	1.0
29.4	190.35	4	10.6	1.0
29.4	188.65	5	16.0	1.0
29.4	188.05	5	16.5	1.0
29.4	184.45	6	40.0	1.0
29.4	183.55	7	54	1.0
29.4	182.05	8	68	1.0
29.4	177.65	9	102	1.0
29.4	176.25	10	116	1.0
29.4	175.75	10	166	1.0
29.6	195.75	0	4.2	1.1
29.6	185.75	5	25.3	1.0

TABLE I—*Continued*

Composition (wt.% NH_3)	Temperature (K)	% Crystallization	Viscosity (poise)	Power law exponent, n
29.6	181.05	8	61	1.1
29.6	176.15	—	488	1.0
33.0	202.25	0	1.7	—
33.0	190.15	0	6.6	1.0
33.0	185.15	0	13.9	1.0
33.0	180.75	0	22.4	1.1
33.0	175.85	—	97	1.0
33.0	176.25	—	78	1.0
33.0	176.15	—	93	1.0
35.5	204.55	0	1.3	—
35.5	200.25	0	1.9	—
35.5	195.85	0	3.2	—
35.5	190.25	0	6.2	1.0
35.5	183.95	0	14.0	1.0
35.5	183.15	0	15.0	1.0
35.5	182.25	0	17.4	1.0
35.5	180.45	0	24.8	1.0
35.5	179.15	0	29.4	1.1
35.5	177.95	0	32.6	1.0
35.5	177.65	0	39.4	—
35.5	176.45	0	35.6	1.0
35.5	175.55	0	43.2	1.0
35.5	173.85	0	50	1.1
35.5	176.45	0	40.0	—
35.5	173.45	0	70	1.0
35.5	171.55	0	74	1.0
42.0	203.35	0	1.2	1.0
42.0	198.45	0	1.9	1.1
42.0	194.25	0	2.9	1.0
42.0	189.45	0	5.3	1.1
42.0	188.75	0	6.4	1.0
49.1	199.35	0	1.2	1.0
49.1	196.75	0	1.6	1.0
49.1	194.85	0	1.8	1.0
57.0	190.65	0	1.1	—
57.0	187.95	0	1.6	1.0

Note. All viscosities were obtained with the HB1 spindle operating at or reduced to 20 rpm. A dashed entry under the crystallization column indicates that partial crystallization occurred at an invariant point preventing use of the lever rule to calculate % crystallization. A dashed entry in the power law exponent column indicates that the data needed to calculate n were not obtained.

a 12.2-cm internal diameter. This vessel was slowly cooled in liquid nitrogen, and was opened for short periods of time to stir and thermally homogenize the liquid, to make viscosity and temperature measurements, and to observe crystallization. The total duration of each run was typically 15 hr, with a mean cooling time on the order of 2–4 K per hour.

Temperature was measured with chromel–alumel thermocouples and platinum resistance thermometers; these instruments were calibrated at the freezing points of water, methanol, and acetone, the sublimation point of carbon dioxide, and the boiling points of nitrogen and water (the latter three temperatures corrected to take into account the laboratory air pressure). The accuracy of the temperature measurements was about ±0.2 K. However, it was difficult to thermally homogenize the more viscous, low-temperature mixtures; this increased the effective temperature error to as much as ±0.5 K for measurements below about 185 K, and ±0.8 K for measurements below 170 K.

2.2. *Falling Sphere Method*

The classical analytical approximation of Stokes gives the viscosity, μ, of a viscous medium if the settling rate of a solid sphere is measured

$$\mu = 2\Delta\rho a^2 g/9U, \tag{1}$$

where $\Delta\rho$ is the density of the solid sphere minus that of the liquid, a is the radius of the sphere, g is the gravitational acceleration, and U is the terminal velocity of the sphere. Equation (1) is a very good approximation if the flow around the sphere is a very slow creeping motion where the Reynolds Number, Re, is much less than 1. Re is given by

$$\mathrm{Re} = 2a\rho_f U/\mu, \tag{2}$$

where ρ_f is the density of the fluid. Various theoretical treatments have offered analytical corrections to the Stokes equation for non-creeping flow at Re of order 1 and higher, although none of these solutions closely reflects reality. Therefore, it is the usual practice to apply empirical corrections. The present data have been reduced according to the empirical correction factors of Le Clair *et al.* (1970). Because the correction factors are Re-dependent and Re is μ-dependent, and μ is not initially known, it was necessary to apply an iterative routine starting with the Stokes approximation to converge on the true, corrected values of Re, the correction factor, and the true, corrected viscosity.

The Stokes Eq. (1) and empirical Re-correction factors apply only in an infinite fluid medium. Rigid boundaries, in this case those of the container, retard the motion of the sinking sphere, so wall corrections must also be applied. The wall effect was accounted for based on the work of Fidleris and Whitmore (1961).

To extend viscosity measurements over many orders of magnitude spheres of various sizes and densities were utilized. These included Cr-steel, glass, nylon, and ultra-high molecular weight polyethylene spheres ranging from 0.6 to 1.3 cm in diameter. Plastics were utilized in the runs at high temperatures in order to minimize the density contrast of the sphere relative to the liquid. Steel and glass were selected to maximize the density contrast for runs

at low temperatures where the liquid became extremely viscous. The temperature-dependent densities of these materials were determined to within ± 0.0004 g cm^{-3}. Small air bubbles sometimes were entrained in the liquid or adhered to the spheres; in some instances this problem may have contributed significant error to measured viscosities.

It was important to thermally equilibrate the sphere with the liquid before measuring its descent rate, both to achieve the correct density contrast with the liquid, and to avoid having the sphere disturb the temperature and viscosity of the sample adjacent to the sphere.

Large hemispherically headed steel bolts, normally used on railroad ties and in wooden bridges, were used in place of spheres to obtain two semi-quantitative viscosity estimates of order 10^6 poises. The effective density of the bolt heads was calculated as the mass of the bolt divided by the volume of a sphere with equivalent cross-sectional area.

The uncertainty in the liquid temperature caused by thermal heterogeneity effectively limited the precision of viscosities measured in excess of about 100 poises. The uncertainties in the density contrasts between the plastic spheres and the viscous media, and the combination of large and somewhat uncertain empirical corrections for the wall effect and finite Re limited the precision of viscosities below about 1 poise. Hence, the falling sphere method yielded its best results between 1 and 100 poises, the same viscosity-temperature-composition region where most rotational viscometric data were obtained. In general, the quality of the falling sphere data is not as good as the quality of the rotational viscometry except near 1 poise. However, the falling sphere method yielded useful results over a broader viscosity range, from 10^{-2} to 10^6 poises.

2.3. Liquid Preparation

The compositional range for the ammonia–water liquids investigated in this study is from about 12.6 to 56.0 wt% NH_3. Ammonia–water solutions with compositions ranging up to 29.9 wt.% NH_3 were prepared by diluting analytical reagent grade ammonium hydroxide (Mallinckrodt, 3 ppm total impurities) with distilled water (maximum 1 ppm impurities). Ammonium hydroxide was precooled to about 260 K to reduce ammonia vapor loss during transfer from the bottle. The composition of the ammonia–water reagent was determined by two independent methods: measurement of the liquid's specific gravity (Croft *et al.* 1988) and measurement of its liquidus temperature.

Solutions with NH_3 contents greater than 29.9% were prepared by mixing ammonium hydroxide solution with anhydrous liquid ammonia (Matheson, maximum 100 ppm total impurities, mostly water); since mixing was done at ambient pressure it was necessary to mix these solutions at low temperatures to prevent boiling. Ammonia was cooled by the Joule–Thompson effect to the normal boiling point (240 K) upon extrusion from the high-pressure cylinder. Ammonia and ammonia–water reagent were then cooled to the freezing point of pure ammonia (196 K) prior to mixing. The quantities of the liquids used in preparing the solutions were measured volumetrically, and their masses were determined using the temperature–composition–density relationship of Croft *et al.* (1988). Determinations of the liquidus temperature before and after experimental runs indicated that ammonia vapor loss and atmospheric water vapor condensation over the course of each run amounted to a reduction of the ammonia concentration from the initial value by about 0.1–0.3%, absolute. The uncertainty in the initial compositions is $\pm 0.2\%$ NH_3. Therefore, one may take $\pm 0.4\%$ as the uncertainty in the liquid composition for a given viscosity measurement. Ammonia–water–methanol liquids were prepared in the same general fashion, using analytical reagent methanol (Mallinckrodt, maximum 0.07% impurities).

3. RESULTS

3.1. Ammonia–Water Liquids above the Liquidus

Figure 1 and Table I show temperature-dependent viscosities of ammonia-water solutions obtained by rotational viscosity. Figure 2 and Table II show the viscosities obtained by the falling sphere method. Figure 2 also shows a curve, discussed below, fit to all superliquidus data obtained in this study (including rotational viscometry) and a fit to the data of Pinevich (1948), both curves for 30% NH_3 solution.

Temperature–composition–viscosity fit. Least-squares numerical fitting procedures (Bevington 1969) were applied to the viscosity measurements to obtain interpolation equations. The basic form of the fitting equation adopted is:

$$\mu = \exp\{A + B/T\}, \tag{3}$$

where μ is the viscosity, T is temperature, and A and B are material constants. The form of Eq. (3) is the one commonly adopted to express viscosity data for both liquids and gases (Touloukian *et al.* 1975), and has both theoretical and empirical support. Effectively, $\exp\{A\}$ is a reference viscosity at very high temperatures and B is an "activation temperature" related to an activation energy. Both A and B vary with ammonia content of ammonia–water liquids, thus in our fit, A and B are represented by polynomial expressions in the mass fraction, X, of ammonia in the mixtures. Both earlier work (McKinnon

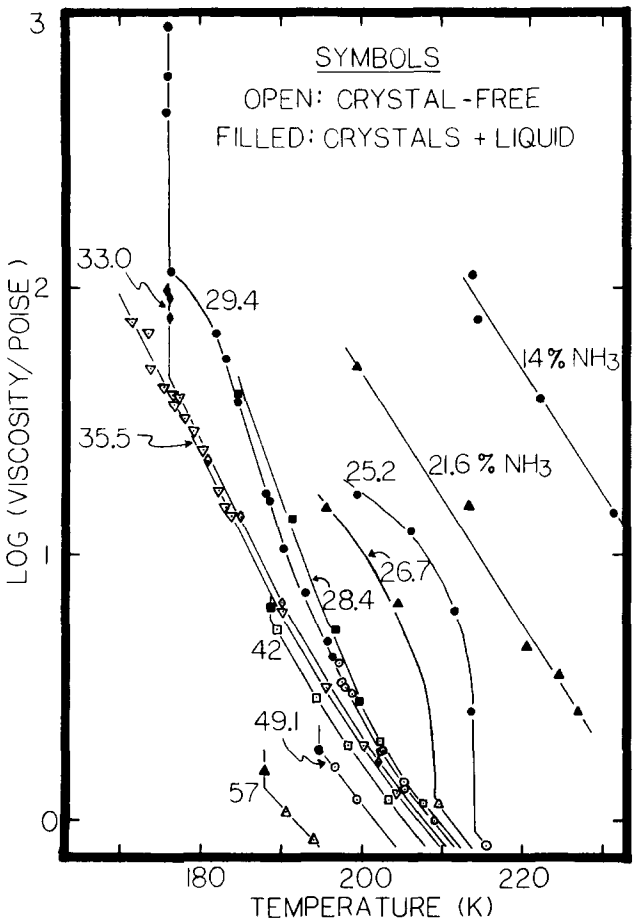

FIG. 1. Effective viscosities of ammonia–water liquids and slurries obtained by rotational viscometry using Brookfield's largest spindle operated at 20 rpm.

and Meadows 1984, Kargel 1987) and our initial attempts to fit both the high-temperature data (Pinevich 1948, Pleskov and Igamberdyev 1939) and our data (Tables I and II) indicated that B was a function of temperature also. Attempts to fit the values of B as a smooth function of temperature were unsuccessful. Measurements bracketing the apparent transition near 240 K indicated a sharp, rather than a gradual transition (Fig. 2). Therefore, two separate fits were made: one to data above 240 K (including the mixed NH_3–H_2O data of Pinevich 1948, and Pleskov and Igamberdyev 1939; pure H_2O data of Haar *et al.* 1984; and pure NH_3 data of Alei and Litchman 1972), and a second to data below 240 K (Tables I and II and supercooled H_2O data from Weast and Selby 1967). The least-squares numerical fits are

$$A = -10.8143 + 0.711062\,X - 22.4943\,X^2 + 41.8343\,X^3 - 18.5149\,X^4 \quad (4a)$$

$$B = 1819.86 + 250.822\,X + 6505.25\,X^2 - 14923.4\,X^3 + 7141.46\,X^4 \quad (4b)$$

for $T > 240$ K, and

$$A = -13.8628 - 68.7617\,X + 230.083\,X^2 - 249.897\,X^3 \quad (5a)$$

$$B = 2701.73 + 14973.3\,X - 46174.5\,X^2 + 45967.6\,X^3 \quad (5b)$$

for $T < 240$ K. RMS deviations from Eq. (4) for the data used in the fit are about 5%. RMS deviations from Eq. (5) for the viscometer data (Table I) used in the fit is about 10%. Deviations of the Stokes Flow data (Table II) from Eq. (5) is about 15%.

Isoviscs computed from Eqs. (3), (4), and (5) are shown in Fig. 3. The computed transition curve between the two solutions is also shown. As with density and bulk modulus (Croft *et al.* 1988), viscosities of ammonia–water liquids show an anomalous maximum near the eutectic composition (see below). Approximate mean activation temperatures are about 2050 K for $T > 240$ K, and about 4200 K for $T < 240$ K. The corresponding activation energies are, respectively, about 17 kJ/mole and 35 kJ/mole, which agree reasonably well with the results of McKinnon and Meadows (1984). Further discussion of this transition is given in Section 4.1.

3.2. *SuperCooled Ammonia–Water Liquids*

The ability to chill liquids below their normal freezing points without crystallization is a common metastable phenomenon (supercooling). The experimentalist must use some measure of patience to prevent significant supercooling of liquids close in composition to the ammonia–water peritectic. In fact, Rupert (1909), in the earliest determination of the complete solid–liquid phase diagram of the ammonia–water system, extrapolated supercooled "liquidus" data from higher temperatures leading to the erroneous conclusion that a eutectic occurred in this system near 158 K, 17 K below the actual value. Several subsequent determinations also erred on the low side.

The correct eutectic composition and temperature (35.4 wt.% NH_3, 175.4 K) and the existence of ammonia dihydrate and of the ammonia–water peritectic (32.6% NH_3, 176.2 K) were first established by Rollet and Vuillard (1956). The early errors, due to strong metastability in the ammonia–water system, have caused a fair amount of confusion in the planetary science community as to the actual minimum melting temperature, with published temperatures of 170, 173, 175, and 176 K. For primitive, previously undifferentiated ammonia–water ices, the actual temperature of melting at low pressures is the peritec-

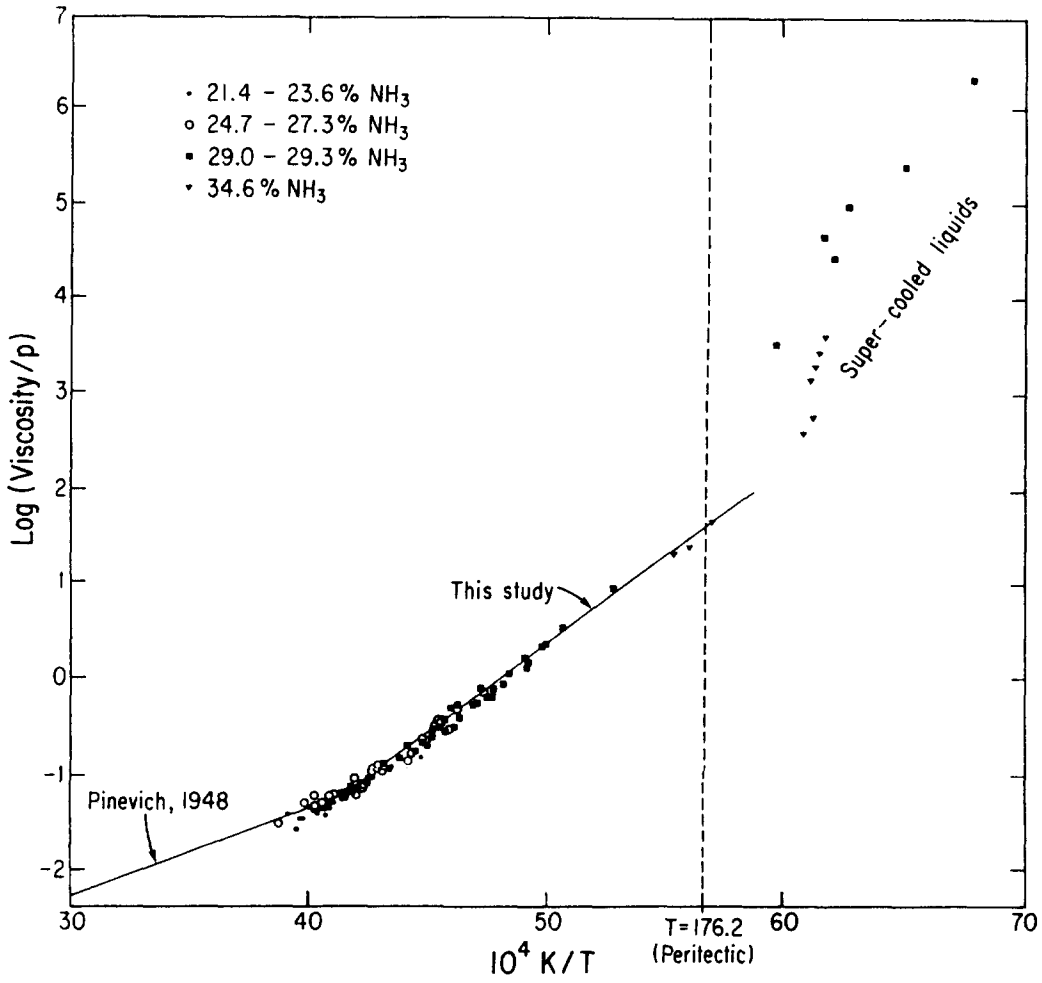

FIG. 2. Viscosities of ammonia–water liquids obtained by the falling sphere method. Curves represent all data obtained by both methods in this study and data of Pinevich (1948).

tic, 176.2 K, rather than the eutectic as is commonly stated. The supercooling phenomenon continues to frustrate many experimentalists when crystallization is desired. However, under certain circumstances supercooling may occur in natural cryovolcanic settings and may be an important factor governing the rheologies of these cryolavas.

Figures 1 and 2 show the viscosities of supercooled ammonia–water liquids near the peritectic in composition. It is possible to maintain ammonia–water liquids several K below the normal freezing point for several hours as long as they are not too vigorously stirred and as long as ice nucleii are not introduced by atmospheric condensation or from moist thermocouple probes or viscometer spindles. It was, therefore, very easy to get good viscosity measurements by either viscometric technique for slightly supercooled liquids.

The more highly supercooled mixtures become highly viscous and thermally inhomogeneous, requiring energetic manual mixing, long thermal equilibration times, or small sample sizes in order to obtain more thermally homogeneous mixtures. Invariably, vigorous manual mixing triggers crystal nucleation within a few minutes, often before the liquid can be thermally homogenized. Sometimes crystallization may be triggered merely by inserting a thermocouple probe or dropping a steel sphere into the liquid. The great difficulty encountered in trying to stir and otherwise manipulate these mixtures severely limited the number and quality of viscosity determinations for highly supercooled mixtures and made them impossible to study by rotational viscometry. The measured viscosities for the strongly supercooled mixtures (Fig. 2 and Table II) were all obtained by the descending sphere method using liquids lacking any observable signs of crystallization. The greatest uncertainty in these measurements is the temperature, which typically varied by 1 K

TABLE II
Viscosities of Ammonia–Water Mixtures Obtained by the Descending Sphere Method

Composition (wt.% NH_3)	Temperature (K)	Stokes viscosity (poises)	Corrected viscosity (poises)
21.4	238.6	0.121	0.069
21.4	239.6	0.117	0.065
21.4	240.0	0.120	0.067
21.4	240.7	0.122	0.069
21.4	241.5	0.144	0.060
21.4	241.5	0.110	0.057
21.4	243.5	0.105	0.052
21.4	244.5	0.098	0.046
21.4	245.6	0.095	0.044
21.4	248.7	0.092	0.042
21.4	251.6	0.085	0.035
21.4	251.7	0.085	0.035
21.4	255.2	0.081	0.038
23.2	234.1	0.162	0.097
23.2	235.3	0.161	0.095
23.2	236.8	0.149	0.084
23.2	237.3	0.136	0.069
23.2	238.0	0.140	0.073
23.2	238.4	0.132	0.065
23.2	240.5	0.124	0.058
23.2	244.6	0.118	0.050
23.2	245.6	0.102	0.038
23.2	247.0	0.110	0.045
23.2	247.6	0.104	0.040
23.6	223.6	0.210	0.146
23.6	230.0	0.180	0.117
23.6	234.1	0.160	0.097
23.6	239.7	0.130	0.065
23.6	249.6	0.112	0.046
23.6	253.3	0.089	0.027
24.7	250.6	0.124	0.052
24.7	244.6	0.134	0.062
24.7	238.0	0.134	0.063
24.7	233.0	0.195	0.121
24.7	225.9	0.241	0.164
24.7	223.4	0.505	0.233
24.7	220.8	0.636	0.334
24.7	219.8	0.665	0.345
25.0	217.8	0.392	0.305
25.0	219.6	0.387	0.295
25.0	234.1	0.183	0.111
25.0	236.4	0.147	0.074
25.0	238.8	0.143	0.070
25.0	248.3	0.120	0.048
25.0	257.9	0.101	0.031
27.3	211.1	1.19	0.715
27.3	216.3	0.866	0.477
27.3	220.1	0.716	0.370
27.3	222.9	0.317	0.225
27.3	226.6	0.220	0.138
27.3	232.0	0.199	0.114
27.3	236.2	0.163	0.080
27.3	238.2	0.179	0.094
27.3	241.3	0.138	0.058
27.3	243.4	0.145	0.063
27.3	246.3	0.134	0.052
27.3	248.3	0.145	0.062
29.0	159.9		102,000 S
29.0	161.5		29,400 S
29.0	162.5		49,500 S
29.0	167.9		3,570 S
29.0	199.9	3.38	2.29
29.0	203.5	1.58	1.31
29.0	206.7	1.35	1.11
29.0	209.3	1.29	0.784
29.0	209.6	0.811	0.658
29.0	210.6	1.11	0.652
29.0	211.9	1.01	0.813
29.0	212.7	0.673	0.538
29.0	213.2	0.660	0.527
29.0	215.8	0.514	0.400
29.0	216.3	0.936	0.530
29.0	217.2	0.409	0.309
29.0	217.5	0.407	0.300
29.0	217.6	0.915	0.497
29.0	219.9	0.449	0.344
29.0	220.1	0.420	0.314
29.0	220.4	0.416	0.315
29.0	221.4	0.331	0.243
29.0	222.5	0.285	0.196
29.0	223.2	0.304	0.221
29.0	225.7	0.254	0.165
29.0	226.8	0.294	0.201
29.0	228.3	0.229	0.146
29.0	232.0	0.216	0.125
29.0	235.9	0.171	0.083
29.0	239.2	0.164	0.075
29.0	241.5	0.155	0.066
29.3	147.7	4,070,000	2,300,000 S
29.3	154.2	481,000	270,000 S
29.3	189.3	9.07	7.89
29.3	197.3	3.72	3.23
29.3	200.1	2.22	1.92
29.3	203.2	1.49	1.28
29.3	203.8	1.70	1.13
29.3	207.7	0.887	0.74
34.6	163.9		1,490 S
34.6	163.3		2,060 S
34.6	162.9		2,850 S
34.6	162.2		4,300 S
34.6	180.6		20.4
34.6	178.6	34.5	24.3
34.6	175.6	68.3	48.0
34.6	164.6	614	412 S
34.6	163.6	893	600 S
34.6	175.8	1025	688 17% crystals
40.4	193.9		5.92
40.4	193.4		5.93
40.4	192.9		5.73

TABLE II—*Continued*

Note. S, supercooled without crystallization. Corrected viscosities have been corrected for the wall effect and finite Reynolds number. The magnitude of the corrections can be assessed by comparison with the Stokes viscosities which have not been corrected.

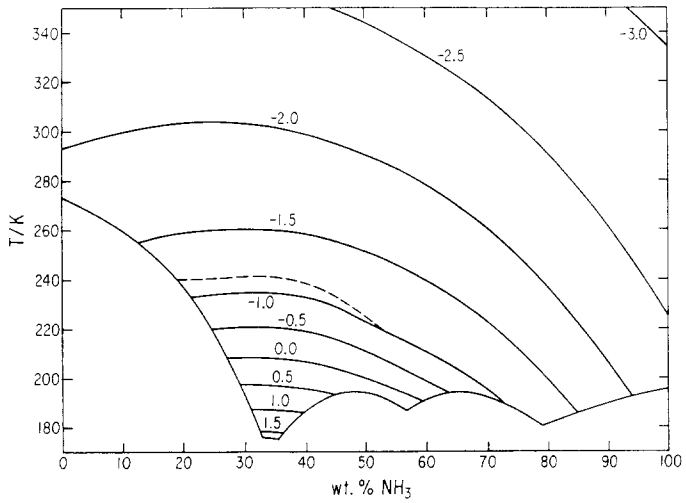

FIG. 3. Temperature–composition–$\log_{10}$ viscosity fit for ammonia–water liquids. Dashed curve shows the transition temperature where the activation energy changes.

through the sample. Considering the sharp temperature dependence of the viscosities in this thermal regime, this introduces a considerable uncertainty in the viscosities for any given temperature.

Figure 2 shows that the viscosities of strongly supercooled ammonia–water liquids exhibit far more powerful compositional and temperature dependencies than do the superliquidus mixtures. This behavior is explained in terms of glass formation in Section 4.1.

3.3. *Partially Crystallized Ammonia–Water Slurries*

Complex rheologies. In contrast to the relatively simply Newtonian viscous behavior of the crystal-free liquids discussed above, partially crystallized slurries are generally characterized by an extremely complex rheology. Even 1 or 2% partial crystallization may introduce a rich variety of rheological phenomena, including hysteresis effects and, most importantly, strain-rate-dependent (shear stress dependent) effective viscosities. The complex rheological behavior of the slurries makes it difficult to exactly reproduce the measured viscosities. For example, the strain rate dependence ensures that the same geometry and shear rate of a viscometric measurement must be reproduced exactly in order to reproduce the same results.

The thermal history also affects the viscosity of ammonia–water slurries. The effective viscosities of well-stirred slurries maintained at constant temperature generally decrease slowly, some tens of percent, over periods of about 10 hr. Part of this phenomenon is probably thixotropy (shear thinning) and is common for particle suspensions in liquids. However, thinning also occurs to some extent for mixtures which are left undisturbed at some constant temperature below the liquidus, and for mixtures which are slightly warmed after cooling without otherwise disturbing them. Such "time-thinning" is probably related to the slow recrystallization of suspended ice, which may initially tend to have dendritic (snowflake-like) forms characteristic of quenched crystals; more compact euhedral and resorbed forms may physically interact less extensively than quenched crystals, for a given crystal packing fraction, therefore yielding lower effective viscosities. To maintain as self-consistent a data set as possible, the effective viscosities of slurries reported in Table I were measured while cooling the mixtures at more or less steady rates.

Simple models of complex rheologies. The rheological behaviors of crystal–liquid suspensions are commonly approximated as "Newtonian" viscous substances, as "power-law" ("pseudo-plastic") substances, or as "Bingham plastics," the latter two comprising common types of non-Newtonian substances. These are sometimes useful approximations to the rheological behavior of naturally occurring slurries (e.g., mud and lava flows), although they often apply only over limited ranges of deformation rates and applied shear stresses.

A Newtonian substance is characterized by a linear dependence of strain rate, $\dot{\varepsilon}$, on applied shear stress, σ, and by the lack of a yield strength. Its viscosity, μ, is defined simply as

$$\mu = \sigma/\dot{\varepsilon}. \tag{6}$$

A Bingham plastic is also characterized by a linear dependence of the strain rate on the applied shear stress, but unlike the Newtonian substance, it also displays a finite yield strength. A Newtonian-like effective viscosity, μ_{eff}, can still be described for a Bingham plastic using Eq. (6), although this effective viscosity varies with the applied shear stress (unlike Newtonian substances). The Bingham viscosity, μ_B, is a constant (for constant temperature) given by

$$\mu_B = (\sigma - Y)/\dot{\varepsilon}, \tag{7}$$

where Y is the yield stress. When $Y \ll \sigma$ a Bingham plastic appears to behave essentially as a Newtonian fluid. When $\sigma < Y$ then no permanent plastic deformation occurs and the substance appears to be an elastic solid.

A pseudoplastic substance lacks a yield strength, and the strain rate has a power-law dependence on the applied shear stress

$$\dot{\varepsilon} = Ae^{-Q/RT}\sigma^n, \tag{8}$$

where A is a constant for a given temperature, Q is the activation energy for viscous flow, and R is the gas constant. The exponential term gives the temperature dependence of the strain rate, and n gives the power-law dependence of the strain rate on the applied shear stress (Newtonian and Bingham substances may have similar temperature dependencies). A value of $n = 1$ signifies Newtonian viscous behavior. As the effective viscosity is simply $\sigma/\dot{\varepsilon}$ (which is constant only in the special case when $n = 1$), we may rewrite Eq. (8) in terms of the effective viscosity,

$$\mu_{\text{eff}} = \sigma^{1-n} e^{Q/RT}/A. \tag{9}$$

Equations (7) and (9) indicate that the effective viscosities of Bingham and power-law substances are functions of the applied shear stress, and in each case give higher effective viscosities as the shear stress and strain rate are decreased. On a graph of strain rate vs shear stress a Newtonian liquid plots as a straight line passing through the origin, a Bingham plastic plots as a straight line with some positive intercept on the shear stress axis, and a power-law substance plots as a curve passing through the origin. In each case the effective viscosity is given by the slope of a straight line passing through the origin and the point of interest on a diagram of stress vs strain rate.

Newtonian character of peritectic slurries. Fortunately, the slurries with the greatest planetological interest (those close in composition to the peritectic) do not exhibit the most troublesome of rheological phenomena (the strain-rate dependence of effective viscosities), so we shall discuss these first.

It is useful to define a relative viscosity, μ_r

$$\mu_r = \mu_s/\mu_l, \tag{10}$$

where μ_s is the viscosity of the slurry, and μ_l is the viscosity of the intergranular liquid phase in the absence of suspended crystals.

Equation (10) has broad relevance only if the slurry is Newtonian. This requirement is satisfied by slurries containing 29% or more NH_3 (at least for the ranges of crystallization and shear rates examined in this work). Figure 4 shows the dependence of μ_r on the percentage of crystals, ϕ, in ammonia–water slurries. ϕ was estimated either by the petrological "lever rule" when there was a reasonably close approach to equilibrium crystallization and when the temperature remained above the peritectic, or by the temperature rise associated with the latent heat released by partial crystallization of supercooled mixtures. μ_s was measured, while μ_l was calculated for the equilibrium liquidus composition at the temperature of the slurry. Like terrestrial lavas, the rheology of ammonia–water liquids is extremely sensitive to its thermal state. Further discussion of this matter is saved for Section 4.2.

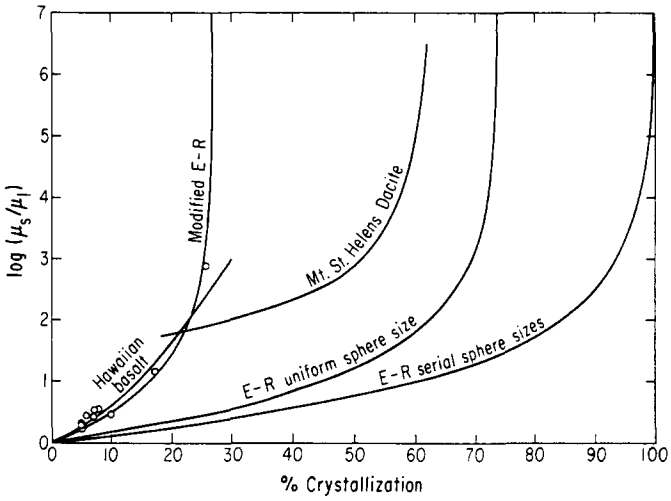

FIG. 4. Dependence of relative viscosity on degree of crystallization. Open circles are ammonia–water slurries. Silicate lava curves are from McBirney and Murase (1984). Theoretical Einstein–Roscoe (E–R) formulations are for uniform solid spheres suspended in a viscous liquid ($C = 1.35$), and for a serial sphere size distribution ($C = 1$), and modified to approximately fit the ammonia–water slurry data ($C = 3.7$).

Figure 5a shows a stress-strain plot for a near-peritectic mixture at various degrees of partial crystallization. No significant departures from ideal Newtonian behavior are discernable. The data can be fit with a power-law where $n = 1$ (the Newtonian condition). A yield strength was not evident for peritectic and near-peritectic mixtures. However, Murase *et al.* (1985) observed an apparent yield strength for Mt. St. Helens dacite only after 70% crystallization. We have not examined slurries with anywhere near this quantity of crystals.

Power-law behavior of water-rich slurries. As the water content of ammonia–water slurries increases from the peritectic their rheologies increasingly depart from Newtonian, with the apparent viscosity describable to a first approximation with a power-law dependence on the strain rate (applied shear stress). Ammonia–water compositions considerably more water-rich than the peritectic were difficult to work with at high degrees of crystallization owing to their strongly non-Newtonian, "slushy" character. At lower degrees of partial crystallization these slurries had a "creamier" consistency and their rheologies were readily studied with the rotational method. The lever rule can be applied to water-rich samples to precisely determine the extent of crystallization as long as the temperature of the slurry remains above the peritectic point.

Figure 5b shows representative stress–strain rate plots obtained for a relatively water-rich mixture at various

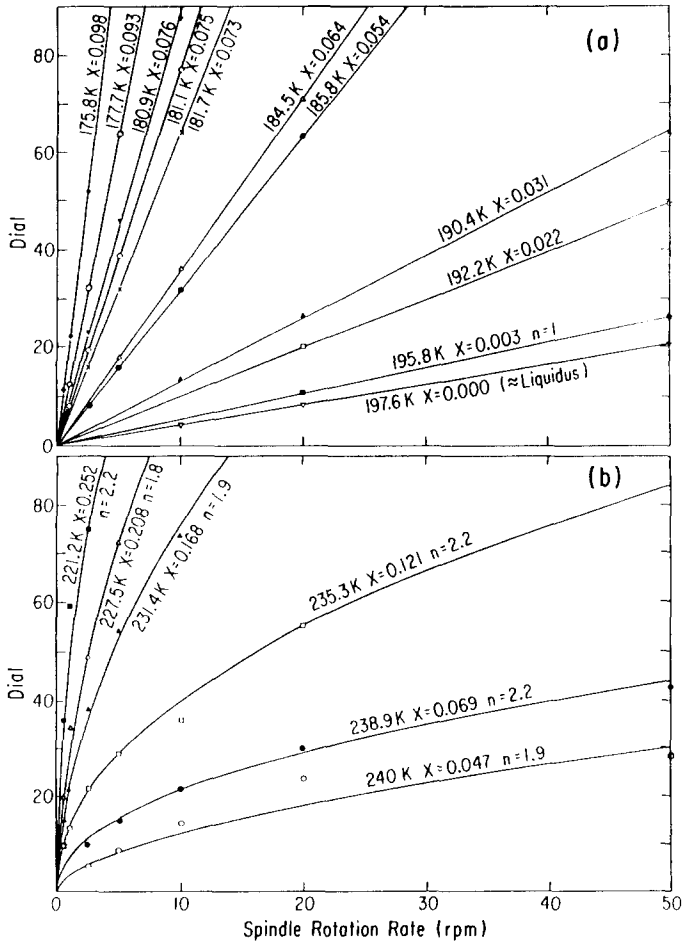

FIG. 5. Strain rate (proportional to spindle rotation rate) vs shear stress (proportional to dial reading). (a) Newtonian behavior of slurries containing 29.4–29.6% NH_3. (b) Power-law pseudo-plastic behavior of slurries containing 18.1% NH_3. X indicates fraction of crystals. n indicates power-law index (equation 8 and Table I).

degrees of partial crystallization. These slurries obey a simple power-law relation to a reasonable approximation. The Bingham approximation completely fails to characterize ammonia–water slurries, at least for the ranges of crystal contents and shear rates investigated here.

Figures 1 and 4 show that abrupt surges in the effective viscosities of water-rich ammonia–water mixtures occur as these substances partially crystallize below their liquidi. Supercooled liquids do not display this phenomenon. This surge in effective viscosity corresponds to the onset of non-Newtonian ($n > 1$) rheological behavior. Figure 6 shows the dependence of the exponent n (from Eqs. (8) and (9)) on the degree of crystallization for several compositions. The exponent n was calculated based on viscosity measurements made at several different spindle rotation rates.

Non-Newtonian power-law viscosities characterize the more water-rich slurries, with n ranging up to about 2. It was surprising to find that n attains its full value with only a few percent crystals, and either levels off or even decreases slightly as the degree of crystallization increases (the effective viscosity, however, certainly does continue to rise sharply as crystallization ensues). This behavior could be a hysteresis effect as described above, where the first few percent of quenched crystals gradually take on more compact, euhedral forms after several hours of slow cooling, thereby minimizing interactions with the liquid and with other crystals.

Although this work does not support a Bingham rheology for ammonia–water slurries, it is possible that such a rheology would be found at a lower range of strain rates or at higher crystal contents than investigated here. Qualitative observations may support this speculation; a stick-slip type of behavior was found for the more water-rich slurries where the ice crystal content exceeded about 25%. That is, the spindle was found to stick and surge in an unpredictable type of rotation. Although this made rheological measurements unreliable, it may indicate that a yield strength was being attained. Alternatively, stick-slip behavior may have been indicating that the spindle was simply cutting a hole in the highly viscous (pseudo-plastic) medium, causing the spindle to surge through free space, followed by the collapse of the sticky material onto the spindle. Or, if the modified Einstein–Roscoe formulation discussed in Section 4.2 is approximately correct, then small heterogeneities in the amount of crystals

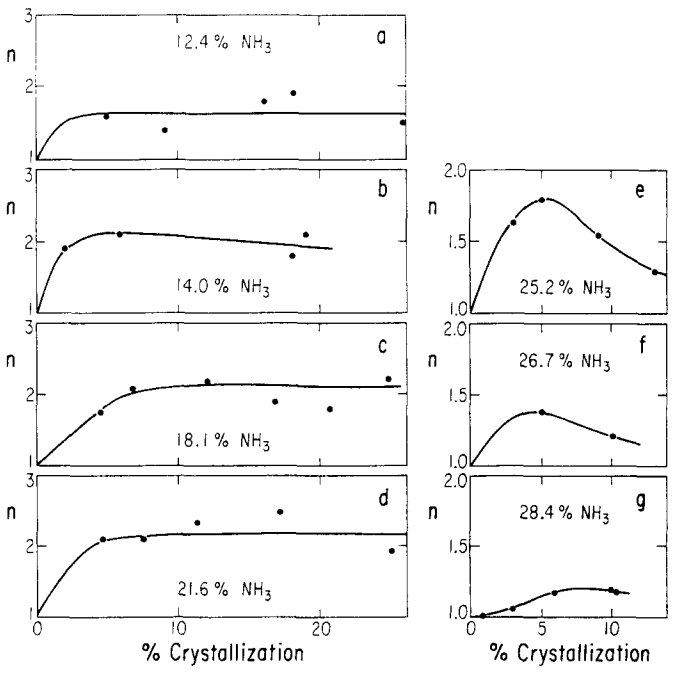

FIG. 6. Strain rate dependence of μ_{eff}, expressed as the power-law exponent n, as a function of the degree of crystallization.

could cause radical local variations in effective viscosity (lumpiness).

3.4. *Ammonia–Water–Methanol Liquids*

Methanol (CH_3OH) is one of the simplest and most abundant organic molecules in interstellar space (Irvine *et al.* 1985) and is readily produced in large quantities by ion bombardments and ultraviolet irradiations of carbon-bearing water ice (Khare *et al.* 1989, Roessler and Nebeling 1988). Methanol and many other molecules may possibly constitute minor or trace components of icy satellites. Since the electric dipole moment of methanol (1.70 D) is similar to the dipole moments of water (1.85 D) and ammonia (1.47 D), we would expect *a priori* that methanol would interact with ammonia–water in extensive liquid solution. Hence, if they are present in at least minor quantities (even hundredths or tenths of 1%) in icy satellites, methanol and other strongly polar substances may contribute to the volcanological complexity and geomorphic diversity of icy satellites (Kargel 1990). This work explores some of the rheological implications when just this one of the many plausible minor components is added to the ammonia–water system.

Kargel (1990) mapped out the liquidus surface of the ternary system H_2O–NH_3–CH_3OH in composition–temperature space at 1 atm. (Fig. 7). The detailed structure of this system, particularly near the methanol corner and near the thermal minima, are known only in approximate form, owing to the difficulty encountered in crystallizing and manipulating these highly viscous mixtures at such low temperatures. The ternary equivalent of the ammonia–water peritectic has been bracketed in temperature–composition space by melting experiments (giving the peritectic temperature) and by extrapolations of the liquidus temperature–composition curves (giving the peritectic composition, and less reliably, the peritectic temperature). The peritectic liquid appears to contain about 33% CH_3OH, 23% NH_3, and 44% H_2O by mass, and apparently freezes near 153 K (all values have large uncertainties at this point).

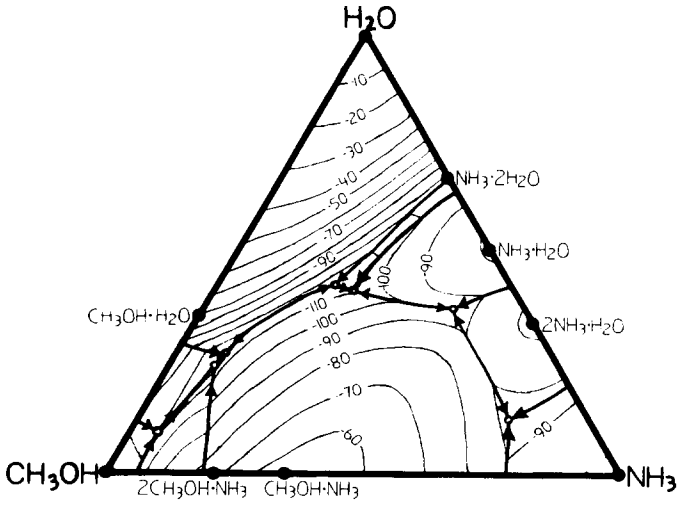

FIG. 7. Liquidus surface of the system H_2O–NH_3–CH_3OH (from Kargel 1990). Isotherms in °C. Arrows on cotectics indicate the direction of liquid migration upon cooling.

TABLE III
Viscosities of Ammonia–Water–Methanol Liquids (by Rotational Viscometry)

Liquid compositions (weight fractions)			Temperature	Viscosity	A	B
H_2O	NH_3	CH_3OH	(K)	(poises)	(Equation (3))	
0.486	0.207	0.307	186.1	26	−34.78	7108.2
			177.4	266		
			167.6	1820		
0.215	0.092	0.693	187.5	1.8	−28.44	5390.6
			179.7	4.3		
			171.1	14.8		
			164.1	75		
			158.0	388		
0.241	0.000	0.759	178.3	2.2	−21.29	3936.9
			168.1	8.4		
0.379	0.090	0.531	198.1	2.7	−31.17	6328.6
			189.9	6.8		
			184.1	20.0		
			177.9	103		
0.442	0.227	0.331	210.7	1.0	−29.80	6188.8
			202.9	2.3		
			201.5	2.9		
			201.2	2.2		
			200.2	3.5		
			198.3	4.6		
			195.8	5.8		
			192.9	7.8		
			192.8	9.0		
			190.7	12.6		
			189.0	17.1		
			185.8	23.6		
			182.0	54		
			177.7	122		
			174.3	320		
			172.2	370		
			170.2	1040		
			165.1	3260		

Table III and Fig. 8 show the viscosities of ammonia–water–methanol liquid mixtures. Some of these mixtures became extremely bubbly at the lower temperatures, and it is possible that the bubbles affected some viscosity measurements. Pure methanol and ammonia end members are less viscous than liquid water for a given temperature. The ternary mixtures, however, are considerably more viscous than simple noninteractive mixing would

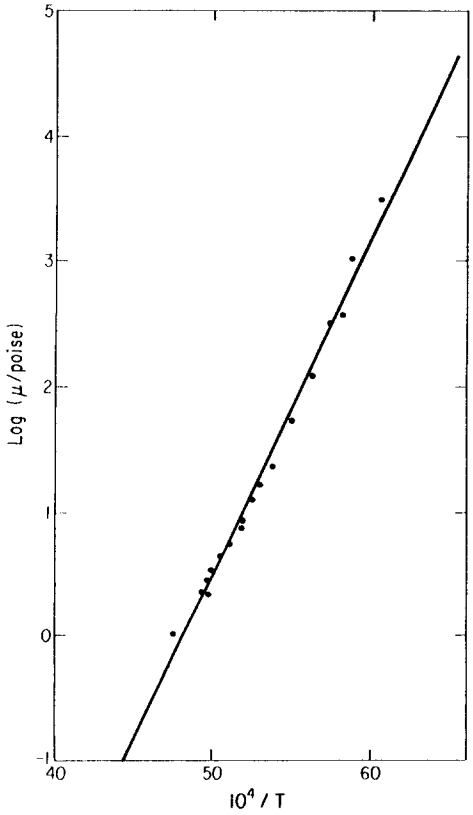

FIG. 8. Viscosities of ammonia–water–methanol liquid (near ternary peritectic) as a function of temperature, obtained by rotational viscometry.

suggest. Hence, powerful molecular interactions among the three components are indicated by the viscosity data.

This inference is supported by the molar volumes of ternary mixtures, which indicate highly nonideal solution behavior and closer intermolecular spacings than in any one of the pure liquids or any of the binary liquid mixtures. For example, the density of a liquid close in comparison to the ternary peritectic ($H_2O:NH_3:CH_3OH$ = 0.470 : 0.201 : 0.329 by mass) is 0.8706 g cm^{-3} at 298 K. This is 6% denser than is calculated based on the densities of the three pure end members and the assumption of noninteractive mixing. It is also 2% denser than calculated from the densities of pure methanol added to ammonia–water liquid assuming no interaction between the methanol and the ammonia–water. Croft *et al.* (1988) had earlier shown that ammonia and water interact strongly in solution. We infer from these density data that methanol interacts strongly with water and ammonia molecules, although less strongly (gram for gram) than the ammonia–water interaction.

The ammonia–water–methanol peritectic mixture has an extraordinarily high extrapolated viscosity near the freezing point, about 4×10^4 poises, three orders of magnitude greater than the viscosity of ammonia–water peritectic liquid (which is itself 3 to 4 orders more viscous than either pure water or pure ammonia at their freezing points). This viscosity estimate is a factor of several uncertain because of the uncertain temperature of the peritectic and because of uncertainties in the extrapolation of the data (a nonlinear fit in Fig. 8 would result in a greater viscosity at the peritectic and reduced rms deviation). The extremely high viscosity of the ternary peritectic compared to the ammonia–water binary peritectic is primarily due to the large additional freezing-point depression imposed by methanol. Ternary molecular interactive forces appear to be secondarily responsible. Just a few percent partial crystallization or a few degrees of supercooling make this mixture impossible to manipulate.

3.5. Comparisons of Planetologically Important Liquids and Ices

Figure 9 shows the viscosities of liquid water, ammonia–water, ammonia–water–methanol, water–magnesium sulfate (Kargel, 1990), and methane–nitrogen (Touloukian *et al.* 1975) mixtures at their respective eutectic and peritectic freezing points. Figure 9 also compares these viscosities to those of common silicate lavas at their liquidus temperatures. The silicate lavas are certainly not plausible volcanic agents on the icy satellites, but are included in Fig. 9 to provide a geologically familiar frame of reference. All of the viscosities shown in Fig. 9 are for crystal-free liquids. Volcanologically realistic amounts of supercooling and partial crystallization can increase these viscosities by many orders of magnitude, as shown in the sections above. Therefore, the viscosities in Fig. 9 are best utilized simply to show the approximate relative differences in the viscosities of the different types of lavas

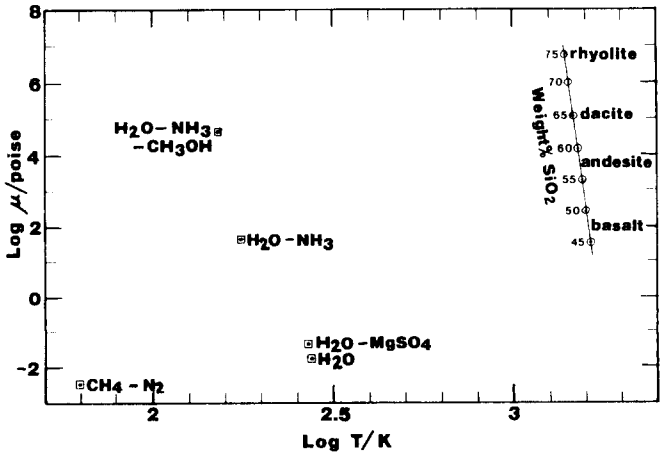

FIG. 9. Viscosities of cryogenic and silicate liquid mixtures. All data are for crystal-free mixtures. Silicates are at their respective liquidi; cryogenic liquids are at their respective eutectic and peritectic points.

FIG. 10. Lab samples of aqueous liquids and slurries of possible cryovolcanic importance. (a) H_2O–NH_3 liquid near the peritectic composition, T = 176 K, 6% ice crystals, ≈100 poises. (b) Supercooled H_2O–NH_3 liquid also containing a few percent ice crystals, T = 160 K, $\approx 10^4$ poises. (c) H_2O–NH_3–CH_3OH peritectic liquid, T = 163 K (about 10 K above peritectic temperature), $\approx 10^4$ poises.

and cryogenic substances. Assuming that superheating of cryolavas above the liquidus is minor or absent (this is true of silicate lavas), then the liquidus viscosities in Fig. 9 correspond to lower limits on the actual eruptive viscosities.

Figures 10a–10c qualitatively illustrate the viscosities of some cryovolcanologically plausible ammonia–water liquids in various thermal states. The ammonia–water–methanol liquid (Fig. 10c) could not be manipulated near its freezing point due to its highly viscous nature, so the experimenter had to settle for a photograph of the sample taken about 10 K above its peritectic temperature.

As seen from Fig. 9 ammonia–water and ammonia–water–methanol peritectic liquids have about the same viscosities as basaltic and dacitic lavas, respectively, and are many orders of magnitude more viscous than pure water, salt brines, or methane–nitrogen mixtures at their respective freezing points.

4. THEORETICAL INTERPRETATIONS AND PLANETOLOGICAL APPLICATIONS

4.1. Theoretical Interpretation of Ammonia–Water Liquid Rheology

Viscosity vs composition. Liquid water is a highly structured phase which, at temperatures well above the freezing point, exhibits some long-range order consistent with the crystal structure of hexagonal ice I (Eisenberg and Kauzmann 1969). Likewise, ammonia, also hydrogen-bonded, exhibits structure in the liquid. It is of interest to understand whether the mixed liquid is ordered, and what the nature of that ordering is. Viscosity data can contribute in this area. In the present section, we interpret the viscosity data as indicating very strongly that the liquid is a mixture of water molecules and ammonia–hydrate and dihydrate molecules, rather than simply free water and ammonia molecules. We also show weak evidence for further structure in the liquid; the following section of viscosity versus temperature provides a more compelling argument for additional structure in the liquid.

In an ideal solution, the viscosities of the two end members characterize the viscosity of the mixture according to the equation (Hummel and Arndt 1985)

$$\log \mu_{\text{mix}} = x \log \mu_y + (1 - x) \log \mu_z, \qquad (11)$$

where μ_y is the viscosity of component y, and x is its mole fraction. In turn, the viscosity of each individual component at temperature T is given by Eq. (3) which can also be written as

$$\mu = \exp\left(A + \frac{B_s}{TS}\right), \qquad (12)$$

where S is the configurational entropy of component x, and A, B_s are constants (compare with Eq. 3). In the case that the solution is not ideal, an additional term is added to Eq. (11) which expresses the contribution of the entropy of mixing of the solution. The notion that the viscosity may be expressed solely in terms of entropy corresponds to the view that material transport in liquids depends on the number of configurations attainable by the system, and that the energy required to shift from one configuration to another is not the rate-limiting step of the transport process. Such a view works well for certain

silicate melts such as plagioclase, even down to the glass temperature (Hummel and Arndt 1985). We adopt this view for our preliminary analysis of the viscosity–composition data and find that it provides a useful perspective.

We assume first that the ammonia–water liquid, above any of the eutectic, peritectic, or congruent melting points, is an ideal mixture of ammonia and water molecules. We then use the fits to the viscosity data given in the previous section to compare the viscosity as a function of composition to that predicted by the ideal mixing equation, with the viscosities of pure water and pure ammonia defining the end members. We use the fits to the data rather than the data themselves because the trends are easier to see using the fits; the goodness-of-fit is thoroughly described above and the reader should refer to this section again before drawing any conclusions.

Figure 11a shows the result of this analysis at 280 K. The solid line is the viscosity; the dashed line is that predicted from ideal mixing. The dashed curve is up to 65% lower in magnitude than the solid line. Discrepancies above the 10 to 20% level are significant, as is the disagreement in the sign of the slope for ammonia mole fractions less that 25%. The direction of the discrepancy is toward a negative entropy of mixing; i.e., the real liquid has fewer configurations available to it than the ideal mixing would predict; hence, the real viscosity is higher than the ideal.

The simplest approach to introducing a restriction in the number of available configurations is to assume that the liquid is composed not of water and ammonia molecules in any configuration, but instead that the molecules are restricted to hydrogen-bonded clusters according to composition. These clusters plausibly correspond to the stoichiometric, solid ammonia hydrate compounds. Thus between mole fractions of 0 and 33% the end member liquid components are H_2O and $2H_2O.NH_3$; between 33 and 50% the end members are $2H_2O.NH_3$ and $H_2O.NH_3$.

Figures 11b and 11c show the results of using the ideal mixing model with the endmember components indicated above. In some sense, the improved agreement is almost a trivial one in that we are taking smaller compositional slices of the viscosity curve in constructing the dashed line, and hence a better fit is to be expected. However, the great improvement in the fit, and the consistency in the sign of the slope, suggest that the result should be regarded as significant. The dashed curve fits the solid curve to within 6% in both the water–dihydrate, and dihydrate–monohydrate regions (Figs. 11b and 11c, respectively). This is much better than the scatter in the data and hence, to within the accuracy of the viscosity data, these dashed, "ideal" curves represent the viscosity data from 0 to 50% ammonia at 280 K. One is tempted to argue that the systematic, small negative residual entropy of mixing suggests additional structure in the liquid, but more accurate data are required to test this assertion.

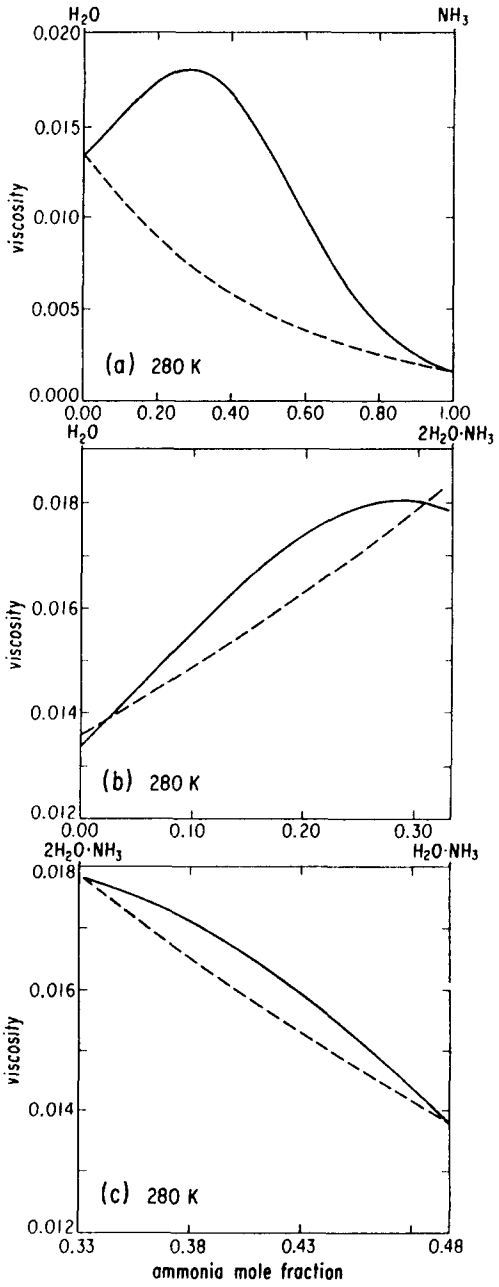

FIG. 11. Viscosity (in poises) versus ammonia mole fraction at 280 K, shown by the solid lines based on fits described in the text. The dashed line in (a) is a model viscosity based on ideal solution of individual ammonia and water molecules. The dashed line in (b) and (c) is a model viscosity based on ideal solution, in which the endmembers represent the compositions of the congruent melting points (or equivalently, the solid hydrates).

We have performed the same test at 220 K, the lowest temperature at which sufficient data are available to make accurate comparisons, and reach the same conclusion. The end member water–ammonia model provides a poor fit to the viscosity data (discrepancies of up to 90%); using

the congruent compositions as end members reduces the errors to 17% or less at 220 K. Note that in this case, we have had to extrapolate the pure water viscosity to well-below the freezing point which undoubtedly introduces additional errors at this low temperature.

The conclusion we draw from Fig. 11 is that the viscosity of the ammonia–water system, well into the liquid regime, can be interpreted in terms of a liquid structure composed of clusters of molecules corresponding to the composition of the solid hydrates (or equivalently the congruently melting end members). Thus from 0 to 33% ammonia, free ammonia molecules do not exist; instead the smallest ammonia unit in the liquid is $2H_2O.NH_3$. From 33 to 50%, the smallest units in the liquid are dihydrate and monohydrate "molecules." Evidence for any additional structure in the liquid which limits accessible configurations is slim or nonexistent. To search for such additional order, higher precision in the data at low temperatures is required. However, additional evidence for order is provided in the following subsection, which treats the dependence of viscosity on temperature.

Viscosity vs temperature. We fitted the viscosity data (for 33% ammonia liquid) with the expression:

$$\mu \alpha \exp(B/T) \tag{13}$$

While in the previous section we argued that the viscosity is given as a function of composition by a composite expression involving at least two terms, we are only interesting here in fixed composition and variable temperature. In effect, we are assigning B to be an "activation energy" (normalized by the gas constant) in the sense of a simple Newtonian fluid, and asking what is its variation with temperature. No more significance than this should be attached to the fit.

The data show two interesting characteristics when fitted to Eq. (13). First, there is a significant change in activation energy at around 240 K, wherein below 240 K $B = 4200$, and above 240 K $B = 2050$ as described in Section 3.1. In both temperature regions B is nearly constant with temperature. Below 176 K, the subcooled liquid has a value of B which increases steeply with decreasing temperature below the peritectic, presaging the onset of glass formation at some lower temperature. The change in activation energy near 240 K suggests a structural change in the liquid involving a loss of attainable configurations at temperatures below the transition. Unfortunately, with the present data, we cannot constrain well the width (in temperature) of the transition; however, we are confident that the data show a discrete rather than gradual change in the liquid structure. The effect is reminiscent of the changes in physical properties which water undergoes as it approaches its freezing point, in which significant long-range order becomes rather established with decreasing temperature (Eisenberg and Kauzmann 1969).

It therefore appears that, in addition to the formation of single-unit hydrate clusters in the liquid over a large range of temperature, some long-range order involving many clusters becomes established at temperatures approaching the congruent melting point of the hydrates. Further investigation of this effect requires higher precision in the viscosity data.

Likewise, the onset of the glass transition is suggested by the peritectic-composition data below 176 K. In this regime the viscosity can be described by an equation which takes account of incipient glass formation at a temperature T_g

$$\mu \propto \exp\left(\frac{+D}{T - T_g}\right), \tag{14}$$

where D is a constant. Preliminary calculations were performed to estimate a glass temperature based on the viscosity data and are in fair agreement with the observed value, measured by Van Kasteren, of 120 K. However, the scatter in the viscosity data permits acceptable fits producing glass temperatures up to 140 K. Therefore, more precise data are required before we can assert with certainty that we are seeing the onset of glass formation in the peritectic liquid.

4.2. Volcanological Implications of Slurry Rheology

Figures 1 and 4 illustrate an important rheological consequence of partial crystallization. The sharp increase in viscosities starting with the onset of crystallization is very similar to that observed for silicate lavas, particularly basalt. However, it is likely that relative viscosities of lavas in general depend not just on the crystal fraction but probably also on the size distribution and form of the crystals. Obviously, skeletal, dendritic, and rodlike crystals would interact differently (more extensively) than spherical or other equant crystals would. Delicate skeletal and rod-like crystallites form when liquid water is quenched (Hobbs 1974) and when water vapor condenses rapidly below the frost point (forming snow and frost). Slow crystallization or recrystallization after rapid precipitation in lavas and glacial ice causes larger, more equant crystal forms to develop so as to minimize the surface area and associated free energy. We expect that a similar behavior would occur in ammonia–water and other aqueous slurries and that this would have rheological effects. Consistent with this idea, we have observed that the viscosity of ammonia–water slurries is somewhat dependent on its thermal history (Section 3.3).

Having expressed our concern that the viscosity of a

particular composition probably depends on much more than just its temperature and crystal content, we can still state with surety that the slurries we examined behaved rheologically very much like silicate lavas. This is not a trivial observation since it is by no means obvious that hydrogen-bonded aqueous mixtures should behave similarly to silicate lavas. The fact that these substances do exhibit similar rheological behavior, at least under the conditions we examined, implies that it is reasonable to interpret cryovolcanic morphologies on the basis of experience gained with terrestrial and extraterrestrial silicate lava flows.

The relative viscosities of ammonia–water slurries and of silicate lavas are much greater than predicted based on Einstein–Roscoe approximations assuming spherical particles (Graham *et al.* 1964). A mere 25% crystallization can increase the viscosities of ammonia–water and silicate slurries by *three orders of magnitude* relative to the homogeneous liquid phase. This increase can be modeled (see "modified E–R" curve in Fig. 4) by a modified form of the Einstein–Roscoe formulation

$$\mu_r = \mu_l(1 - C\phi)^{-2.5}, \tag{15}$$

where the coefficient C is assigned a value of 3.7 (this compares to $C = 1.35$ for uniform spheres traveling in aggregates). C physically represents the increased effectiveness of highly aspherical crystals and crystal aggregates in blocking much of the liquid volume from participating in the deformation of the slurry.

According to Eq. (15), $C = 3.7$ means that a slurry would behave as a solid when ϕ attains a value near 30% crystals (compared to about 70% crystals for uniform spheres where $C = 1.35$, and 100% crystals for a serial distribution of sphere sizes where $C = 1$). Possibly this is the critical crystal fraction when a basalt or ammonia–water slurry attains a yield strength, or at least appears to have one. Below this critical crystal fraction, where all of our measurements were made, we observed a Newtonian rheology for near-peritectic slurries, and a power-law rheology for water-rich slurries (Section 3.3).

Even in the total absence of a yield strength the effective cessation of motion of a cooling flow could be quite abrupt, occurring when the chilled flow front and margins crystallize the critical volume fraction of solids. When this happens the viscosity of the chilled crust of the flow increases sharply, even as the less crystallized interior slurry maintains a relatively low viscosity. This effect could be approximated with a Bingham rheology involving a yield strength. However, on the basis of our experiments and the data of others (e.g., Shaw 1969, and Murase *et al.* 1985), we suspect that the commonly utilized Bingham model is simply a convenient way to approximate thermally and rheologically heterogenous flows having power-law rheologies. The final dimensions of lava flows depend on the dynamical problem of the characteristics of the eruptive event, the viscous run-out of the flow, and the cooling behavior of the flow margins. Any true yield strength probably does not appear until the final moments when the lava flow has already virtually attained its final shape. This could explain the widely observed correlation between lava viscosity (and composition) and apparent yield strength (McBirney and Murase 1984, Murase *et al.* 1985, Fink and Zimbelman 1986, Moore and Ackerman 1989). Nevertheless, the yield strength concept is widely used among volcanologists, and we feel that it does provide useful results.

4.3. Cryolava Rheology and Comparative Planetology

Surface gravity is probably one of the more important variable parameters affecting the evolution and appearance of planets and satellites. Of present concern are the effects that intersatellite variations in surface gravity may impose on the dimensions and morphologies of cryovolcanic flows. Variations in lava viscosity affect lava flow morphology opposite to variations in the product of lava density and surface gravity. This is evident, for example, in problems dealing with Newtonian flow down an inclined plane or channel flow (Turcotte and Schubert 1982). Since simple rheological models of lava flows often seem to give incorrect results (evidently because the dynamical rheological structures of lava flows are not simple!), we find it easiest and safest to perform a first-order gravity scaling of cryogenic liquids so as to arrive at a gravity-scaled rheological analog among terrestrial lavas. Based on simple flow models we define a "mobility index" = $\log_{10}(\rho g/\mu)$. Liquids with the same mobility index should, to a reasonable approximation, behave in rheologically similar ways.

Figure 12 shows the mobility indices of silicate and cryogenic liquids plotted against surface gravity. Obviously our choice of plotting parameters ensures that there will be a positive correlation with a slope of unity. The purpose of this figure is simply to provide a visual guide for rheological gravity scaling.

For example, from Fig. 12 we see that liquid water and salt brines on Ganymede would be about 10 times "runnier" than the most fluid lavas (komatiite) on Earth, thus probably producing submeter flow thicknesses on Ganymede. Mixtures of nondipolar molecules such as methane and nitrogen on Triton would be even more fluid. Ammonia–water on Enceladus should be roughly comparable to andesite on Earth, perhaps producing flows on the order of a few tens of meters thick on low slopes. Ammonia–water–methanol on Miranda or Ariel should behave like rhyolite on Earth, producing flows up to several hundred meters thick on low slopes.

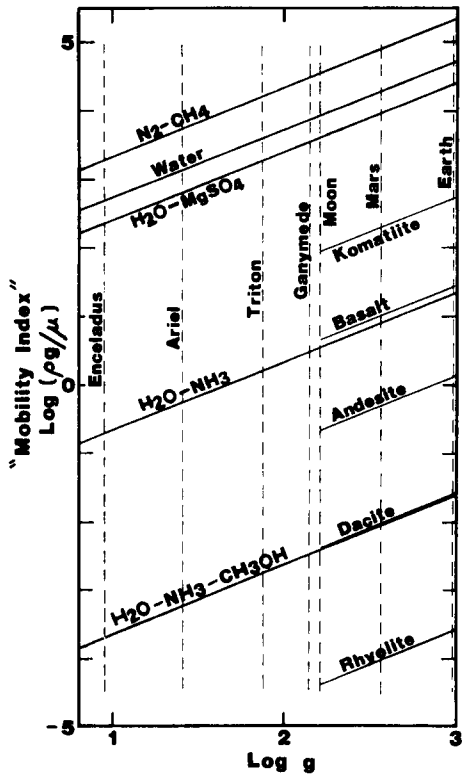

FIG. 12. Gravity-scaling of viscosities of volcanic and cryovolcanic liquids. In each case the viscosity at the freezing point (liquidus) and in the absence of suspended crystals is represented. Data for volatile mixtures are the eutectic and peritectic compositions. Silicate lava viscosities are from the first author's compilation of experimental data for natural and synthetic rock compositions, and the temperatures for which these viscosities apply are the eutectic temperatures in synthetic water-free multicomponent mixtures approximating natural rock compositions (Morse 1980).

Another important aspect illustrated by Fig. 12 is that while intersatellite variations in surface gravity may be an important variable factor controlling surface morphologies, cryolava compositions are far more important if these compositions vary significantly through the outer Solar System.

4.4. Observed Cryovolcanic Morphologies

The observed morphologies of volcanic deposits on the terrestrial planets have been used to place crude constraints on the magma rheologies (e.g., Pieri and Baloga 1986, Dragoni *et al.* 1986, Fink and Bridges 1990, and references therein). The techniques are admittedly imperfect, but seem to give reasonable results. Not all of the techniques can be applied to flows on the icy satellites because not all of the morphologic features found on terrestrial flows are seen on the ice flows, probably because of the generally poor resolution (order 1–10 km) of available images of icy satellite cryovolcanic deposits. A few techniques are useful, however. Fink (1980) presented a theory from which the internal viscosity of a volcanic flow can be estimated from the amplitude and wavelength of drag folds (corda or festoons) on the flow surface, when present. Hulme (1974) presented a method of estimating the yield strength of a flow from the height and curvature of the flow's convex or lobate edge. Since effective yield strengths seem to correlate with viscosities, the latter gives a qualitative estimate of viscosities as well. Assuming that these techniques can be applied to deposits on the icy satellites, the observed morphologies imply a broad range of effective viscosities at the time of emplacement for deposits on various satellites.

The coronal deposits on the Uranian satellite Miranda are interpreted as cryovolcanic flows (Croft 1987, 1988) with lobate edges hundreds of meters thick and surface ripples with amplitudes of hundreds of meters and wavelengths of a few kilometers. Assuming the ripples are corda, internal viscosities of 10^8–10^9 poise are obtained. The lobate deposit dimensions imply yield stresses of 0.01–0.1 bar. Both measurements are consistent with each other and imply rheologies comparable to terrestrial andesites. On Ariel, there are long linear and lobate flows with convex edges on the order of a kilometer high, implying yield strengths on the order of a bar. No corda are visible, but comparison with the inferred yield strength indicate probable viscosities in the range of 10^{10} poise. These high viscosities imply that the erupted substances on Miranda and Ariel were composed of some low-melting-temperature aqueous mixture, probably involving several chemical components and perhaps a high degree of crystallinity. High as they are, these viscosity estimates are orders of magnitude below the 10^{16} poises obtained by Jankowski and Squyres (1988) for the flows on Ariel. Straightforwardly interpreted viscosities of this order would suggest that the flows were erupted as solid ice (as the title of their paper indicates) rather than as volcanic slurries. However, Jankowski and Squyres pointed out that their viscosities are upper limits, and considered alternatives to solid ice including ice mobilized by interstitial cryogenic liquids. Jankowski and Squyres' models assumed a homogeneous and purely viscous rheology, and did not adequately consider the critically important rheological effects of the chilled crust of the flows on their mobility. Following Greenberg *et al.* (1990) and Schenk (1989), who suggested that a 4–6 order-of-magnitude crust correction factor must be applied to the results of simple flow models, we consider (on the basis of Jankowski and Squyres' uncorrected results) that eruptive viscosities on the order of 10^{10}–10^{12} poises are more likely for Ariel, and an order of magnitude less for Miranda, in rough agreement with the results based on corda and yield strengths.

Neptune's large satellite Triton has both flat deposits

with no discernable lobate edges and thick, lobate flows and ridges. The former are apparently low-viscosity deposits, possibly like those on Enceladus and Tethys, whereas the latter are high viscosity deposits with rheologies comparable to the stiff flows on Ariel and Miranda (Kargel and Strom 1990).

Several Saturnian satellites show evidence of resurfacing. Most spectacular are the broad, smooth plains of Enceladus. These plains are nearly featureless at the best image resolutions (2 km per line-pair), except where they are interrupted by arcuate and linear ridges (Squyres *et al.* 1983, Pozio and Kargel 1989). The lack of obvious flow margins and fronts in these plains, coupled with the very low surface gravity of Enceladus, indicates that the cryovolcanic liquids must have possessed much lower viscosities than the substances which formed the lobate deposits on the Uranian and Neptunian satellites. However, considering the limitations of image resolution, substances as viscous as ammonia–water are allowed.

Another large cryovolcanic plain is found on Tethys to the east of Ithaca Chasma. The plain is recognizable in contrast to the rugged cratered terrain due to its flat surface and somewhat lower crater density. The western boundary of the plain with the cratered terrain is very irregular (Moore and Ahern 1983) and suggests flooding of the rugged upland to a constant topographic level. There is no visible raised edge to the plains deposit, again suggesting a relatively low viscosity at the time of emplacement.

Another style of cryovolcanism is seen on Ganymede, the largest of the icy satellites. Its surface consists of moderately cratered dark plains and light, grooved, smooth materials. The light materials were early recognized to be cryovolcanic deposits on the basis of age, stratigraphy, and embayment relationships (e.g., Lucchitta 1980, Head *et al.* 1981, Parmentier *et al.* 1982). The rougher dark plains were later recognized to consist of a complex of darker cryovolcanic flows based again on embayment patterns, age relationships, and albedo variations (Casacchia and Strom 1984, Croft 1985, 1986). The edges of the light deposits are generally defined by tectonic structures. In the few cases where embayment relations are not tectonically disturbed, there is little or no evidence for a raised edge where topographic variations on the order of 100 m would easily be seen. The boundaries of albedo patches within the dark terrain (which presumably represent individual flows or distinct groups of flows) range from relatively sharp to quite diffuse. The highest resolution images show little or no vertical definition to the edges of the albedo patches or to the smooth dark patches within the dark terrain (interpreted as local flooding by Casacchia and Strom 1984), again where topographic variations of 100 m would be visible. The thinness of the flows and the general lack of definable flow edges indicate low viscosity flows with maximum yield stresses of 0.01–0.1 bar, and probably much less. The flows may have been emplaced as liquid water, slush, or brine with viscosities of 10^{-2} poise, although ammonia–water cannot be ruled out based on the available data. Observations by Galileo will place firmer bounds on the rheology and composition.

The cryovolcanic surfaces seen on the icy satellites vary enormously in their morphologies, and accordingly we infer a great range in their rheological properties at the times of eruption. These properties are nonetheless within the range of viscosities for likely cryomagma compositions. In particular, the higher inferred viscosities on the icy satellites can easily be reached by partially crystallized cryogenic binary materials such as ammonia–water or by cryogenic ternary mixtures, while very water-rich substances, salt brines, or ice-free ammonia–water can explain the lower inferred viscosities. A direct correspondence between composition and morphology is not justifiable, because the inferred differences in rheology may be (and probably are) due to differences in eruption temperatures and crystallinity of the cryomagmas as well as differences in composition. In addition, pressure is an important variable affecting liquid compositions and cryovolcanic rheologies (Cynn *et al.* 1989; Hogenboom and Kargel, 1990), although we have not explicitly considered such effects to date. Beyond these uncertainties, we find it intriguing that the more fluid cryolavas were erupted on the satellites of Jupiter and Saturn, while the more viscous cryolavas were erupted on the satellites of Uranus and Neptune.

5. SUMMARY

Cryovolcanic deposits have been observed on many of the icy satellites. We have gathered relevant viscosity data from the literature and have performed new viscosity measurements on a number of theoretically plausible cryomagma compositions. The compositions included binary and ternary mixtures of water, ammonia, and methanol, both as liquids and as partially crystallized slushes. The viscosities of one-component liquids are orders of magnitude too fluid to account for many of the flows, particularly those any with discernable thickness. Binary mixtures of liquid water and ammonia have substantially higher viscosities, up to 100 poise, enough to account for many of the observed flows. The thickest observed flows require the much higher viscosities that are only reached in our experiments by ternary mixtures or partially congealed binary mixtures. Collectively, these materials can account for all observable flows; thus, we find no justification for postulating solid-state extrusion.

These experiments point out the importance of mixtures of simple compounds that provide a difference in temperature between the solidus and liquidus in allowing the complex behavior of real extrusive materials, whether on the

terrestrial planets or on the icy satellites. Our experiments are still only an initial foray into the complexity of materials and material properties that almost certainly exists on the icy satellites, complexity that must be taken into account as more detailed models of their structure and history are constructed.

ACKNOWLEDGMENTS

We thank Robert Strom for many constructive discussions related to this work. Special thanks to Jay Melosh who kindly loaned us his Brookfield viscometer. J.I.L. acknowledges support from NASA Grant NAGW-1039; S.K.C. and J.S.K. from NSG-7146; and J.S.K. and J.S.L. from NHGW-340.

REFERENCES

ALEI, JR., M., AND W. M. LITCHMAN 1972. Density and viscosity of liquid ND_3. *J. Chem. Phys.* **57,** 4106–4110.

BEVINGTON, P.R. 1969. *Data Reduction and Error Analysis for the Physical Sciences,* McGraw-Hill, New York.

CASACCHIA, R., AND R. G. STROM 1984. Geologic evolution of Galileo Regio, Ganymede. *Proc. Lunar Planet. Sci. Conf. 14, part 2, J. Geophys. Res. (Suppl.)* **89,** B419–B428.

CONSOLMAGNO, G. J., AND J. S. LEWIS 1978. The Evolution of Icy Satellite Interiors and Surfaces. *Icarus* **34,** 280–293.

CROFT, S. K. 1985. A new scenario for differentiation of Ganymede and Callisto. *Lunar Planet. Sci. XVI,* 152–153.

CROFT, S. K. 1986. Ganymede and Callisto: Toward a new synthesis. *Rep. Planet. Geol. Geophys.—1895,* NASA TM 88383, 57–59.

CROFT, S. K. 1987. Miranda geology and tectonics: A non-catastrophic interpretation. *Lunar Planet. Sci. XVIII,* 207–208.

CROFT, S. K. 1988. Miranda's Inverness Corona interpreted as a cryovolcanic complex. *Lunar Planet. Sci. XIX,* 225–226.

CROFT, S. K., J. I. LUNINE, AND J. S. KARGEL. 1988. Equation of state of ammonia–water liquid: Derivation and planetological application. *Icarus* **73,** 279–293.

CYNN, H.-C., S. BOONE, A. KOUMVAKALIS, M. NICOL, AND D. J. STEVENSON 1989. Phase diagram for ammonia–water mixtures at high pressure: Implications for icy satellites. *Proc. Lunar Planet. Sci. Conf., 19th,* pp. 433–441.

DRAGONI, M., M. BONAFEDA, AND E. BOSCHI 1986. Downslope flow models of a bingham liquid: Implications for lava flows. *J. Volcanol. Geotherm. Res.* **30,** 305–325.

EISENBERG, D., AND W. KAUZMANN 1969. *The Structure and Properties of Water.* Oxford Univ. Press, New York.

FIDLERIS, V., AND R. L. WHITMORE 1961. Experimental determination of the wall effect for spheres falling axially in cylindrical vessels. *Brit. J. Appl. Phys.* **12,** 490–494.

FINK, J. 1980. Surface folding and viscosity of rhyolite flows. *J. Volcanol. Geothermal Res.* **8,** 250–254.

FINK, J., AND N. BRIDGES 1990. Predicting extra-terrestrial lava flow morphology. *Lunar Planet. Sci. XXI,* 363–364.

FINK, J. H., AND J. R. ZIMBELMAN 1986. Rheology of the 1983 Royal Gardens basalt flows, Kilauea Volcano, Hawaii. *Bull. Volcanol.* **48,** 87–96.

GRAHAM, A. L., R. D. STEELE, AND R. B. BIRD 1964. Particle clusters in concentrated suspensions. 3. Prediction of suspension viscosity. *Ind. Eng. Chem. Fundam.* **23,** 420–425.

GREENBERG, R., S. CROFT, D. JANES, J. KARGEL, L. LEBOFSKY, J. LUNINE, R. MARCIALIS, H. MELOSH, G. OJAKANGAS, AND R. STROM 1991. Miranda, in *Uranus* (J. Bergstralh and M. S. Matthews, Eds.). Univ. of Arizona Press, Tucson. In press.

HAAR, L., J. S. GALLAGER, AND G. S. KELL 1984. *NBS/NRC Steam Tables.* Hemisphere Pub. Corp. New York.

HEAD, J. W., M. L. ALLISON, E. M. PARMENTIER, AND S. W. SQUYRES 1981. High-albedo terrain on Ganymede: Origin as flooded graben. *Lunar Planet. Sci. XII,* 418–420.

HOBBS, P. V. 1974. *Ice Physics.* Oxford Univ. Press.

HOGENBOOK, D. L., AND J. S. KARGEL 1990. Ammonia–water densities and phase relations to four kilobars. *Lunar Planet. Sci. XXI,* 522–523. [Abstract]

HULME, G. 1974. The interpretation of lava flow morphology. *Geophys. J. R. Astron. Soc.* **39,** 361–383.

HUMMEL, W., AND J. ARNDT 1985. Variation of viscosity with temperature and composition in the plagioclase system. *Contrib. Mineral. Petrol.* **90,** 83–92.

IRVINE, W. M., F. P. SCHLOERB, A. HJALMARSON, AND E. HERBST 1985. The chemical state of dense interstellar clouds: An overview. In *Protostars and Planets II.* (D. E. Black and M. S. Matthews, Eds.), pp. 579–620. Univ. of Arizona Press, Tucson.

JANKOWSKI, D. G., AND S. W. SQUYRES 1988. Solid-state ice volcanism on the satellites of Uranus. *Science* **241,** 1322.

KARGEL, J. S. 1987. Density and Viscosity Measurements of NH_3–H_2O Liquids. *Lun. Planet. Sci. XVIII,* 475–476. [Abstract]

KARGEL, J. S. 1988. Liquidus phase relations and liquid properties in the system H_2O–NH_3–CO_2–H_2CO. *Lun. Planet. Sci. XX,* 583–584. [Abstract]

KARGEL, J., AND R. STROM 1990. Cryovolcanism on Triton. *Lun. Planet. Sci. XXI,* 599–600. [Abstract]

KARGEL, J. S. 1990. *Cryomagmatism in the Outer Solar System,* Ph.D. dissertation, Univ. of Arizona, Tucson, 309 pages.

KHARE, B. N., W. R. THOMPSON, B. G. J. P. T. MURRAY, C. F. CHYBA, C. SAGAN, AND E. T. ARAKAWA 1989. Solid organic residues produced by irradiation of hydrocarbon-containing H_2O and H_2O/NH_3 ices: Infrared spectroscopy and astronomical implications. *Icarus* **79,** 350–361.

LE CLAIR, B. P., A. E .HAMIELEC, AND H. R. PRUPPACHER 1970. A numerical study of the drag on a sphere at low and intermediate reynolds numbers. *J. Atmos. Sci.* **27,** 308–315.

LEWIS, J. S. 1972. Low temperature condensation from the solar nebula. *Icarus* **16,** 241–252.

LUCCHITTA, B. K. 1980. Grooved terrain on Ganymede. *Icarus* **44,** 481–501.

MCBIRNEY, A. R., AND T. MURASE 1984. Rheological properties of magmas. *Annu. Rev. Earth Planet. Sci. 1984,* 337–357.

MCKINNON, W. B., AND M. MEADOWS 1984. Rheological measurements of ammonia–water melt. *Bull. Amer. Astron. Soc.* **16,** 686. [Abstract]

MOORE, H. J., AND J. A. ACKERMAN 1989. Martian and terrestrial lava flows. *Lun. Planet. Sci. XX,* 711–712. [Abstract]

MOORE, J. M., AND J. L. AHERN 1983. The geology of Tethys. *Proc. Lunar Planet. Sci. Conf. 13th, Part 2, J. Geophys. Res. Suppl.* **88,** A577–A584.

MORSE, S. A. 1980. *Basalts and Phase Diagrams.* Springer-Verlag, New York.

MURASE, T., A. R. MCBIRNEY, AND W. G. MELSON 1985. Viscosity of the dome of Mount St. Helens. *J. Volcanol. Geotherm. Res.* **24,** 193–204.

PARMENTIER, E. M., S. W. SQUYRES, J. W. HEAD, AND M. L. ALLISON 1982. The tectonics of Ganymede. *Nature* **295,** 290–293.

PIERI, D., AND S. M. BALOGA 1986. Eruption rate, area, and length relationships for some Hawaiian lava flows. *J. Volcanol. Geotherm. Res.* **30,** 29–45.

PINEVICH, G. 1948. Viscosity of ammonia–water solutions and of liquid ammonia. *Kholodil. Tekh.* 20(3), 30–37. [In Russian]

PLESKOV, V. A., AND I. IGAMBERDYEV 1939. Viscosity of mixtures of ammonia and water at 20°C. *J. Phys. Chem. (USSR)* **13,** 701–702.

POZIO, S., AND J. S. KARGEL 1989. The tectonic and igneous evolution of Enceladus. *Lunar Planet. Sci. XX,* 864–865.

ROESSLER, K., AND B. NEBELING 1988. High energy and radiation chemistry in space. *Lunar Planet. Sci. XIX,* 994–995. [Abstract]

ROLLET, A. P., AND G. VUILLARD 1956. Sur un novel hydrate de l'ammoniac. *C.R. Acad. Sci. Paris* **243,** 383–386.

RUPERT, F. F. 1909. The solid hydrates of ammonia. *J. Amer. Chem. Soc.* **31,** 866–868.

SCHENK, P. 1989. Fluid volcanism on Miranda and Ariel. *Lunar Planet. Sci. XX,* 958–959. [Abstract]

SHAW, H. R. 1969. Rheology of basalt in the melting range. *J. Petrol.* **10,** 510–535.

SQUYRES, S. W., R. T. REYNOLDS, P. M. CASSEN, AND S. J. PEALE 1983. The evolution of Enceladus. *Icarus* **53,** 319–331.

TOULOUKIAN, Y. S., S. C. SAXENA, AND P. HESTERMANS 1975. Viscosity of liquids and liquid mixtures. In *Thermophysical Properties of Matter.* Vol. 11. Viscosity, pp. 33–46. Plenum, New York.

TURCOTTE, D. L., AND G. SCHUBERT 1982. *Geodynamics: Applications of Continuum Physics to Geological Problems.* Wiley, New York.

VAN KASTEREN, P. H. G. 1973. The crystallization behavior and caloric properties of water/ammonia mixtures between 70 and 300 K. *Bull. Inst. Froid. Annexe* **4,** 81–87.

WEAST, R. C., AND S. M. SELBY 1967. *Handbook of Chemistry and Physics.* 48th ed., Chemical Rubber Co., Cleveland.